International Journal of Control, Automation, and Systems 21(2) (2023) 339-349
http://dx.doi.org/10.1007/s12555-021-0915-1
ISSN:1598-6446 eISSN:2005-4092
http://www.springer.com/12555

LPV Model-based Adaptive MPC of an eVTOL Aircraft During Tilt Transition Subject to Motor Failure

Shen Qu, Guoming Zhu*, Weihua Su, and Sean Shan-Min Swei

Abstract: This paper applies novel LPV (linear parameter-varying) model and MPC (model predictive control) methods to a tilt-transition process with rotor failure for electric vertical take-off and landing aircraft of six distributed electric rotors with a fixed-wing for level flight, where two rotors are tiltable to generate variable thrust vector during the tilt-transition from hovering to steady-state level flight and the rest of four cannot be tilted. During the level flight, the aerodynamic lift induced by fixed wing maintains flight altitude. Based on a predefined nominal tilting trajectory scheduled by tilt-rotor angular position and the failed rotor speed, a discrete-time LPV model is constructed based on significantly reduced number of linear time invariant models obtained by linearizing the nonlinear eVTOL aircraft model along the tilting trajectory, where tilt-rotor angle and failed rotor speed can be measured in real-time. An LPV modeling error evaluation method is proposed based on the σ shifted $\mathcal{H}_2$ norm, and adaptive model predictive controller is designed with the dynamic reference compensation. Simulation study indicated the success of the adaptive MPC strategy based on tilt-transition LPV model with rotor failure.

Keywords: Adaptive MPC, electric virtical take-off and landing (eVTOL), linear parameter-varying (LPV), tilt-transition control, tilt-transition failure control.

1. INTRODUCTION

An eVTOL aircraft equipped with a distributed electric propulsion (DEP) system has proven to have potential to transform future air travel within the city and between suburb and city. The key enabling technologies for this disruptive travel method are due to many recent technological advancements on, for instance, high-density battery, power electronics, composite materials and structural design method, high-throughput real-time computing, etc. On the other hand, there are still many technical challenges to be overcome; see Uber Elevate's 2016 White Paper [1]. One of the most promising eVTOL platforms is the hybrid eVTOL aircraft platform that combines VTOL capability utilizing multi-rotor DEP system with aerodynamic efficiency of the fixed-wing aircraft. There are many eVTOL literature such as market prediction for emerging needs [2], planning eVTOL route and trajectory [3-6], aircraft dynamics and control analysis [7], energy modeling and its optimization [8-13], and failure analysis [14]. Many eVTOL aircraft prototypes were developed and flight-tested. For instance, Joby S2/S3, Boeing Swift, Airbus Vahana, Lilium Jet, and Hyundai/Uber S-A1, to just list a few. Note that these eVTOL aircraft rely on DEP thrust vectoring to make flight mode transition from hovering to level flight, and vice versa.

For aircraft with tiltable rotors, the transition from hovering to level flight mode can be achieved by tilting propellers from vertical (tilt-up) to the forward position (tilt-forward), and as a result, the level flight speed increases from zero to the desired cruising speed correspondingly. Noting that modeling the transition process is challenging since it deals with nonlinear parameter-varying aircraft dynamics in multiple dimensions. For this study, the target aircraft has two side-by-side tiltrotors. This configuration has been widely studied in aerospace research. In [15], the operational mode transition of XV-15 tiltrotor aircraft was based on a time-varying linear model and control. Adaptive model inversion control is studied in [16] to reduce control development time and improve closed-loop system performance. Also, aircraft with four synchronously tilting rotors is presented in [17,18]. However, compared with many existing studies in the area of tiltrotor aircraft transition control with number of rotors less than or equal to four for existing eVTOL prototypes, this paper deals with these aircraft with a large number of distributed rotors. For example, Joby S4, Uber eCRM-001 and Solvay VA-1X have six, six, and eight rotors, respectively. Also,

Manuscript received November 3, 2021; revised February 16, 2022; accepted March 23, 2022. Recommended by Associate Editor Jongho Shin under the direction of Editor Chan Gook Park.

Shen Qu and Guoming Zhu are with the Department of Mechanical Engineering, Michigan State University, East Lansing, Michigan 48824, USA (e-mails: {qushen, zhug}@msu.edu). Weihua Su is with the Department of Aerospace Engineering and Mechanics, The University of Alabama, Tuscaloosa, Alabama 35487-0280, USA (e-mail: suw@eng.ua.edu). Sean Shan-Min Swei is with the Department of Aerospace Engineering, Khalifa University, Abu Dhabi, 11111, UAE (e-mail: sean.swei@ku.ac.ae).
* Corresponding author.

it is worth mentioning that not all rotors need to be tiltable due to the following two reasons. Firstly, the vertical thrust required for maintaining hovering is always much larger than the longitudinal thrust required for holding the desired cruising speed and altitude, which means that only part of rotors needs to be tilted. Secondly, minimizing the weight added by the tilting mechanism leads to using minimal number of tiltrotors possible. For example, the Uber eCRM-001 and Solvay VA-1X have two and four tiltable rotors with six and eight rotors in total, respectively. The LPV-based flight mode transition control of a six-rotor aircraft with two tilt-rotors was studied in [19].

This paper studies the six-rotor eVTOL aircraft developed earlier [20], where the middle two rotors are tiltable, and the two-front and two-rear ones are fixed vertically. A 2-D LPV model [21-23] describing the aircraft transition process was developed along the given tilt-transition trajectory and failed rotor speed. In many existing LPV aircraft modeling literature, trimming the nonlinear aircraft model at multiple equilibrium conditions to obtain a set of linear time-invariant (LTI) models and then linking these LTI models to form one LPV model is a proven technique; see [24,25]. However, for modeling the tilting transition process with rotor failure, this method results in significant modeling error due to the assumption of unrealistic zero aircraft acceleration during the tilt transition. In this research, trajectory linearization method was adopted to further reduce the LPV modeling error, where a number of linearized time invariant models were obtained using trajectory linearization instead of steady-state linearization to form an 1-D LPV model. Note that for the aircraft with motor failure during tilt transition, there are varying parameters, tilt angle and failed rotor speed, which requires extremely high number of linearized models to form a 2-D LPV model with very large memory size. In this paper, it is proposed to develop the 2-D LPV model based on the 1-D (tilt angle) nominal tilt transition with analytically linearized term, updated online, as function of failed rotor speed; see Subsection 2.4 for details.

To utilize the developed 2-D aircraft LPV model, the adaptive model predictive control (MPC) method [26-29] is proposed for control design based on tilt-transition LPV model with motor failure due to its capability of hard constraint handling [30-32]. Since MPC relies on a specific set of weightings to achieve desired performance, to improve the control system performance with reduced real-time calculation throughput, a few changes are made for MPC including feedback dynamic reference compensation and utilization of real-time varying weightings and constraints. The designed adaptive MPC strategy was evaluated using the nonlinear rigid-body eVTOL model in Matlab/Simulink.

This paper's main contributions can be summarized in two-fold: development of the online updated 2-D LPV tilt-trasition model with motor failure and application of adaptive MPC for handling hard control constraints with dynamic reference compensation.

This paper is organized as follows. Section 2 provides a brief review of the nonlinear rigid-body dynamics for the target hybrid eVTOL aircraft and the 2-D LPV modeling method, along with model error evaluation using σ shifted $\mathcal{H}_2$ norm; and Section 3 conducts a modeling error study for the developed 2-D LPV model. Section 4 studies the adaptive MPC design based on given time-varying weightings and hard constraints with two dimensional parameters; and simulation study is conducted in Section 5 to demonstrate the proposed mode transition control scheme. Conclusions are drawn in Section 6.

2. 2D-LPV AIRCRAFT TRANSITION MODEL WITH ERROR EVALUATION

2.1. Nonlinear aircraft model

Fig. 1 shows the proposed eVTOL aircraft configured with two tilt-rotors, where ρ denotes the tilt angle. In [20] a nonlinear rigid-body dynamic model was developed by incorporating tilt-rotor dynamics and their gyroscopic coupling effects. In addition to the control surfaces of a fixed-wing aircraft, the distributed rotor rotational speeds and the tilt-rotor angular position are also considered as control inputs. Table 1 contains the relevant component properties for the eVTOL aircraft considered in this study. Note that when the two mid-rotors tilt forward, there are certain air flow interferences to both front and rear rotors. However, since the two outside rotors are tiltable, it is expected that the air flow interferences are relatively small and in this model this effect is omitted. Furthermore, development of control-oriented model with detailed air flow dynamics is challenge, especially for low-order control-design models.

By following the Hamilton's Principle, the coupled

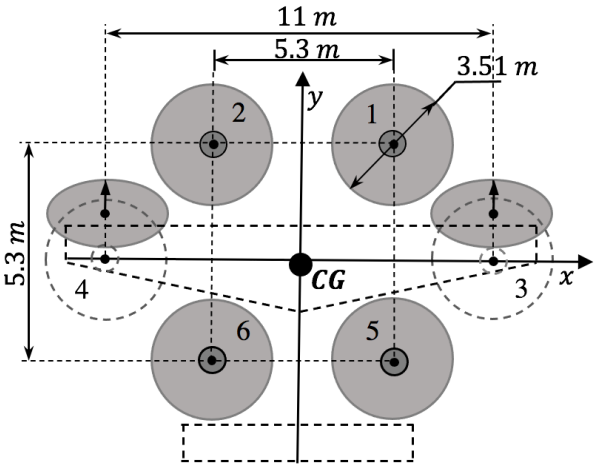

Fig. 1. Geometry of UAM aircraft.

Table 1. Inertial properties of eVTOL aircraft.

Parameter name	Value	Unit
Body mass, m_B	2240.73	kg
Body moment of inertia, $\mathbf{I}_{B,xx}$	12000	kg m^2
Body moment of inertia, $\mathbf{I}_{B,yy}$	9400	kg m^2
Body moment of inertia, $\mathbf{I}_{B,zz}$	20000	kg m^2
Rotor mass, m_r	4.55	kg
Rotor moment of inertia, $\mathbf{I}^e_{r,xx}$	3.5	kg m^2
Rotor moment of inertia, $\mathbf{I}^e_{r,yy}$	7.0	kg m^2
Rotor moment of inertia, $\mathbf{I}^e_{r,zz}$	3.5	kg m^2

Table 2. Definitions of eVTOL system inputs and states.

Input	Definition
Front R/L rotor acceleration	u_1/u_2
Mid R/L rotor acceleration	u_3/u_4
Rear R/L rotor acceleration	u_5/u_6
Ruddervator deflection	u_7
Mid R/L rotor tilt acceleration	u_8/u_9
System State	Definition
Rigid-body velocity	x_1 to x_6
Euler angle	x_7 to x_9
Body inertial position	x_{10} to x_{12}
Propeller speed	x_{13} to x_{18}
Mid R/L rotor tilt angle	x_{19} to x_{20}
Mid R/L rotor tilt rate	x_{21} to x_{22}

fixed-wing and tilt-rotor dynamics can be given below; see [20] for details.

$$\mathbf{M}_{BB}(\rho)\dot{\beta}+\mathbf{C}_{BB}(\beta,\rho)\beta=\mathbf{R}_B, \tag{1}$$

where β denotes the aircraft rigid-body velocity, $\mathbf{M}_{BB}$ the inertia matrix, ρ the tilt angle, $\mathbf{C}_{BB}$ the damping matrix, and $\mathbf{R}_B$ the external loads that include, for instance, gravity, gyroscopic, propulsive, and aerodynamics loads. Moreover, equation (1) together with rotational and translational kinematics completely describe the nonlinear tilt-rotor flight dynamics, as shown in [20]. To design the adaptive MPC strategy, this nonlinear eVTOL model is linearized for a given tilt-trajectory to obtain a two-parameter LPV state-space model. To be specific, the eVTOL aircraft system inputs and states are as listed above in Table 2.

2.2. Linearization along the nominal trajectory

Based on a predefined aircraft transition trajectory, consider a state-space nonlinear aircraft model described below

$$\dot{x}(t)=f(x(t),u(t)), \tag{2}$$

where f is differentiable with respect to state vector $x(t)\in\mathbb{R}^{n_x}$ and control input vector $u(t)\in\mathbb{R}^{n_u}$. It is assumed that $x(t)=x_0(t)+\Delta x(t)$ and $u(t)=u_0(t)+\Delta u(t)$, where the pair $(x_0(t),u_0(t))$ denote the nominal state and control vectors, respectively, and pair $(\Delta x(t),\Delta u(t))$ small deviations of state and input vectors from the nominal condition. Also, $x_0(t)$ and $u_0(t)$ satisfy the nonlinear state equation

$$\dot{x}_0(t)=f(x_0(t),u_0(t)), \tag{3}$$

as a result, (2) can be reorganized as follows:

$$\dot{x}_0(t)+\Delta\dot{x}(t)=f(x_0(t)+\Delta x(t),u_0(t)+\Delta u(t)). \tag{4}$$

Conducting the Taylor series expansion to the above yields

$$\begin{aligned}\dot{x}_0(t)+\Delta\dot{x}(t)=f(x_0(t),u_0(t))+\mathcal{A}\Delta x(t)+\mathcal{B}\Delta u(t)\\ +\Psi_f(\Delta x(t),\Delta\dot{x}(t),\Delta u(t)),\end{aligned} \tag{5}$$

where matrices $\mathcal{A}$ and $\mathcal{B}$ are the sensitivity ones for the nominal conditions, and Ψ_f is the collection of high-order negligible terms. Substituting (3) into (5) results in

$$\Delta\dot{x}(t)=\mathcal{A}\Delta x(t)+\mathcal{B}\Delta u(t). \tag{6}$$

Assuming that system output $y(t)$ is linear with respect to system states, (6) can be organized as following since $\Delta\dot{x}(t)=\dot{x}(t)-\dot{x}_0(t)$.

$$\begin{cases}\dot{x}(t)=\dot{x}_0(t)+\mathcal{A}\Delta x(t)+\mathcal{B}\Delta u(t),\\ y(t)=Cx(t).\end{cases} \tag{7}$$

The above equation can be discretized with a given sampling time T as below

$$\begin{cases}x(k+1)-x_0(k+1)=\dot{x}_0(k)T+A\Delta x(k)+B\Delta u(k),\\ y(k)=Cx(k),\ \ k=0,\ 1,\ \ldots,\end{cases} \tag{8}$$

where (A,B) are the discrete-time system matrices derived from $(\mathcal{A},\mathcal{B})$ with a given sample time T, and $x_0(k)$ and $\dot{x}_0(k)$ are the nominal state vector and its derivative at time step k, respectively.

2.3. Affine form of LPV model

Linearly interpolating the time-invariant state-space models at two adjacent operational conditions along a nominal tilt-trajectory over a varying parameter (or scheduling parameters) to obtain an LPV model can be found in [33]. Assuming that the tilt-rotor angular position $\rho(t)$ is measurable in real-time, a family of M linearized system models can be obtained along the given nominal tilting trajectory, covering the start to end of tilting process with ρ as the scheduling parameter. This set of linear models can be defined as

$$\begin{cases}x(k+1)=x_0^i(k+1)+\dot{x}_0^i(k)T+A^i\Delta x(k)\\ \qquad\qquad +B^i\Delta u(k),\\ y(k)=Cx(k),\end{cases} \tag{9}$$

where $i = 1, 2, ..., M$ denotes the i-th linearized model at the i-th tilt position ρ^i; and matrices A^i and B^i are associated system and input matrices of the linearized model. As a result, the discrete-time affine LPV model can be put into the following form,

$$\begin{cases} x(k+1) = x_0(\rho(k+1)) + \dot{x}_0(\rho(k))T \\ \qquad\qquad + A_\rho(\rho(k))\Delta x(k) + B_\rho(\rho(k))\Delta u(k), \\ y(k) = Cx(k), \end{cases} \tag{10}$$

where $\Delta x(k) = x(k) - x_0(\rho(k))$ and $\Delta u(k) = u(k) - u_0(\rho(k))$, and system matrices $A_1(\rho_1(k))$ and $B_1(\rho_1(k))$ are given by

$$\begin{aligned} A_\rho(\rho(k)) &= A^i + (A^{i+1} - A^i)\frac{\rho(k) - \rho^i}{\rho^{i+1} - \rho^i}, \\ B_\rho(\rho(k)) &= B^i + (B^{i+1} - B^i)\frac{\rho(k) - \rho^i}{\rho^{i+1} - \rho^i}, \\ \rho(k) &\in [\rho^i, \rho^{i+1}],\ i = 1,\ 2,\ ...,\ M-1. \end{aligned} \tag{11}$$

Parameter $\rho(k+1)$ in (10) cannot be measured at time step k but it is needed for real-time control. Note that if the sampling rate is sufficiently high, the difference between $\rho(k+1)$ and $\rho(k)$ is very small. Therefore, it is reasonable to assume that $\rho(k+1) \approx \rho(k)$ with a very small sample period T. As a summary, the resulting LPV model is an approximation of nonlinear aircraft dynamics along the desired operational trajectory using one parameter $\rho(k)$. For this study, sampling period T is 1 msec.

2.4. 2-D linearization with motor failure

Noting that when the aircraft is operated under full or partial motor failure condition, the maximum motor power available for the failed motor will be reduced down to the corresponding level of failure. For instance, if one third of the motor is failed due to shorted winding, the maximum motor power available will be reduced down to $2P_{hmax}/3$, where P_{hmax} is the maximum available power for a healthy motor. In this case, if the desired motor power is higher than the available, after the motor is failed, its rotor speed will be reduced from its nominal (trimmed) condition, which means the locally linearized 1-D LPV model is no longer accurate and a 2-D LPV model as function of tilt angle and failed rotor speed vector is needed to model the aircraft accurately. Note that the failed rotor speed vector $\dot{\Gamma}$ can be measured directly used as a scheduling parameter.

Following the same principle of generating the 1-D LPV model in a normal tilt-transition, one option is to linearize the nonlinear aircraft model under all operational conditions. However, it leads to an exponentially increasing number of offline linearized models due to increased dimension. For example, consider obtaining 20 LTI models of a single rotor failure at each trimmed condition along the transition trajectory with 20 trimmed points, it requires 400 LTI models to be saved in the real-time controller to form the 2-D LPV model, which requires fairly larger memory. Thus, in this subsection, a novel 2-D LPV model is proposed based on the nominal 1-D LPV transition model with online adaptive parameters.

Based on the nonlinear aircraft model (1), a linearization equation can be expressed as

$$(.)\Delta\dot{\beta} + (.)\Delta\beta = \left.\frac{\partial \mathbf{R}_B(\dot{\Gamma})}{\partial \dot{\Gamma}}\right|_0 \Delta\dot{\Gamma} + (.), \tag{12}$$

where β is the aircraft rigid-body velocity, $\mathbf{R}_B$ is total load applied to the aircraft and $\dot{\Gamma}$ denotes the speed vector of six rotors. Notation $(.)$ presents the omitted linearization terms which are not effected by the variation of rotor speed. Applied load $\mathbf{R}_B$ consists of $\mathbf{R}_B = \mathbf{R}^{\text{grav}} + \mathbf{R}^{\text{iner}} + \mathbf{R}^{\text{rate}} + \mathbf{R}^{\text{gyro}} + \mathbf{R}^{\text{prop}} + \mathbf{R}^{\text{aero}}$, where only terms of gyroscopic load $\mathbf{R}^{\text{gyro}}$ and proposive load $\mathbf{R}^{\text{prop}}$ are correlated with the propeller speed $\dot{\Gamma}$ as below.

$$\left.\frac{\partial \mathbf{R}_B(\dot{\Gamma})}{\partial \dot{\Gamma}}\right|_0 = \left.\frac{\partial \mathbf{R}^{\text{gyro}}(\dot{\Gamma})}{\partial \dot{\Gamma}}\right|_0 + \left.\frac{\partial \mathbf{R}^{\text{prop}}(\dot{\Gamma})}{\partial \dot{\Gamma}}\right|_0, \tag{13}$$

where proposive load is formulated as

$$\mathbf{R}^{\text{prop}} = (.)\mathcal{F} + (.)\mathcal{T}. \tag{14}$$

Noting that $\mathcal{F}$ and $\mathcal{T}$ are the thrust and torque applied to the rotors that can be calculated by

$$\mathcal{F} = C_T \rho A \dot{\Gamma}^2 R^2, \quad \mathcal{T} = k\dot{\Gamma}^2, \tag{15}$$

where C_T, ρ, A and k are constant coefficients. Based on (14) and (15), $\mathbf{R}^{\text{prop}}$ can be converted to a proportional form of $\dot{\Gamma}^2$ as $\mathbf{R}^{\text{prop}} = K\dot{\Gamma}^2$, which means $\left.\frac{\partial \mathbf{R}^{\text{prop}}(\dot{\Gamma})}{\partial \dot{\Gamma}}\right|_0 = 2\dot{\Gamma}K$. As for the gyroscopic load $\mathbf{R}^{\text{gyro}}$, based on the calculation from target aircraft specification parameters, it has been observed that the gyroscopic load $\mathbf{R}^{\text{gyro}}$ is much smaller than the external load $\mathbf{R}^{\text{prop}}$ due to slow tilting speed. Thus, by omitting the effects from the variation of term $\mathbf{R}^{\text{gyro}}$, the rotor speed dependent term $\left.\frac{\partial \mathbf{R}_B(\dot{\Gamma}_0)}{\partial \dot{\Gamma}}\right|_0$ in (12) can be approximated by

$$\left.\frac{\partial \mathbf{R}_B(\dot{\Gamma})}{\partial \dot{\Gamma}}\right|_0 = \left.\frac{\partial \mathbf{R}_B(\dot{\Gamma}_0)}{\partial \dot{\Gamma}}\right|_0 \left(\frac{\dot{\Gamma}}{\dot{\Gamma}_0}\right), \tag{16}$$

where $\left.\frac{\partial \mathbf{R}_B(\dot{\Gamma}_0)}{\partial \dot{\Gamma}}\right|_0$ and $\dot{\Gamma}_0$ are the offline linearized system parameter and rotor speed along the nominal trajectory. In this way, the 2-D LPV model can be formulated based on the 1-D nominal LPV model, with the rotor speed dependent system parameters online identified based on the rotor speed vector $\dot{\Gamma}$. Converted from the nominal transition LPV system stated in (10), the 2-D LPV model can

be put into the following form

$$\begin{cases} x(k+1) = x_0(\rho(k+1)) + \dot{x}_0(\rho(k))T \\ \qquad\qquad + A(\rho(k), \dot{\Gamma}(k))\Delta x(k) \\ \qquad\qquad + B(\rho(k), \dot{\Gamma}(k))\Delta u(k), \\ y(k) = Cx(k), \end{cases} \tag{17}$$

where C is defined as an identity matrix since all the state signals are measurable. Note that the LPV system model matrices A and B are not constant and are affine functions of two scheduling parameters: aircraft tilt angle ρ and failed rotor speed deviation vector $\Delta\dot{\Gamma}$. The varying system matrices enable the MPC control to adapt to the failed rotor dynamics to improve the closed loop system performance. In summary, for modeling the aircraft transition process with motor failure, this 2-D LPV model is constructed based on the nominal transition LPV model scheduled by the rotor tilt angle ρ, where part of the LPV system model is identified online as a function of rotor speed $\dot{\Gamma}$.

3. EVALUATION OF 2-D LPV MODEL ERROR

Considering a 2-D LPV model interpreted based on the nominal transition LPV model, the 2-D LPV model error can be evaluated using the eigenvalues of system matrix A, and analyzing the natural mode variation between every two adjacent models. However, system input matrix B is not considered in this case, which means the sensitivity of control efforts is ignored. Thus, a model error evaluation method is introduced in this section using σ-shifted $\mathcal{H}_2$ norms.

3.1. σ-shifted $\mathcal{H}_2$ norm of a system

For a stable, proper single-input and single-output (SISO) system with a transfer function $G(s)$, the $\mathcal{H}_2$ norm is defined by

$$\left\|G(s)\right\|_2 = \sqrt{\frac{1}{2\pi}\int_{-\infty}^{\infty} |G(j\omega)|^2 d\omega}. \tag{18}$$

Assuming that the realization of $G(s)$ is $\dot{x} = Ax + Bu$ and $y = Cx$, a deterministic interpretation of $\mathcal{H}_2$ norm can be obtained from its impulse response $g(t)$ below

$$\left\|G(s)\right\|_2 = \sqrt{\int_0^{\infty} |g(t)|^2 dt} = \left\|g(t)\right\|_2, \tag{19}$$

where $g(t) = Ce^{At}B$ denotes the system impulse response.

Last but not the least, define $g(t) = [g_1(t), g_2(t), ..., g_{n_u}(t)]$, where $g_i(t)$ is the i-th impulse response with respect to the i-th input and n_u is number of inputs, and the $\mathcal{H}_2$ norm of the MIMO system is defined by

$$\left\|G(s)\right\|_2 = \sqrt{trace\int_0^{\infty} g^T(t)g(t)dt}. \tag{20}$$

Since $g(t) = Ce^{At}B$ in Eq. (20), the square of the $\mathcal{H}_2$ norm is

$$\begin{aligned} \left\|G(s)\right\|_2^2 &= trace\int_0^{\infty} B^T e^{A^T t} C^T C e^{A} t B dt \\ &= traceB^T \int_0^{\infty} e^{A^T t} C^T C e^{A} t dt B. \end{aligned} \tag{21}$$

Letting

$$P = \int_0^{\infty} e^{A^T t} C^T C e^{A} t dt, \tag{22}$$

leads to

$$\left\|G(s)\right\|_2 = \sqrt{traceB^T PB}, \tag{23}$$

where $P \geq 0$ is the solution of the following Lyapunov equation

$$A^T P + PA + C^T C = 0. \tag{24}$$

Noting that $trace(MN) = trace(NM)$ for two matrices M and N with compatible dimensions, Eq. (21) can be rewritten as

$$\left\|G(s)\right\|_2^2 = trace\int_0^{\infty} Ce^{At} BB^T e^{A^T t} C^T dt, \tag{25}$$

and the $\mathcal{H}_2$ norm can also be expressed as

$$\left\|G(s)\right\|_2 = \sqrt{traceCP_cC^T}, \tag{26}$$

where $P_c = \int_0^{\infty} e^{At} BB^T e^{A^T t} dt \geq 0$ is the solution of the following Lyapunov equation

$$AP_c + P_c A^T + BB^T = 0. \tag{27}$$

Noting that the $\mathcal{H}_2$ norm is defined for stable systems. However, for an LTI system model, there may be some unstable modes. To handle this situation, a relative stability principle is introduced here by shifting the imaginary axis to the right by σ amount, which converts the original unstable modes to stable ones for σ-shifted $\mathcal{H}_2$ norms denoted by $\mathcal{H}_{\sigma-2}$ for future model error evaluation. For a system $G(s)$, the $\mathcal{H}_{\sigma-2}$ is defined by

$$\left\|G(s)\right\|_{\sigma-2} = \left\|G(s+\sigma)\right\|_2 = \sqrt{trace(CP(\sigma)C^T)}, \tag{28}$$

where $P(\sigma) \geq 0$ is obtained by solving the following Lyapunov equation

$$(A - \sigma I)P(\sigma) + P(\sigma)(A - \sigma I)^T + BB^T = 0. \tag{29}$$

3.2. Model error evaluation

Recalling the $\mathcal{H}_{\sigma-2}$ norm introduced in the previous subsection and assuming that all the modes are well aligned, the model error between the exact trimmed linear model $G_{trim}(s)$ under desired rotor failure condition and

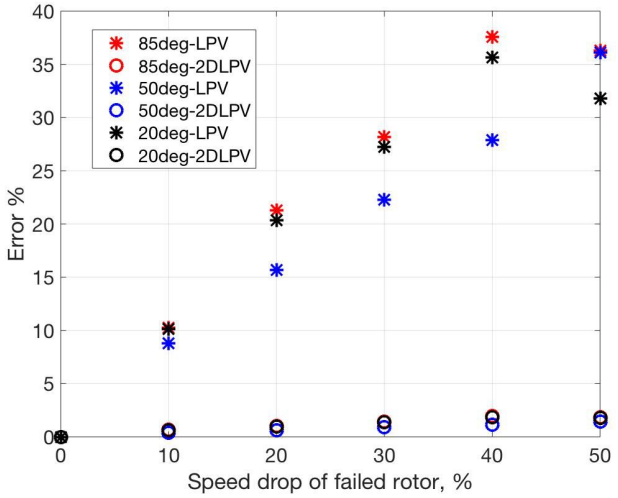

Fig. 2. Model error evaluation with front-right rotor failure.

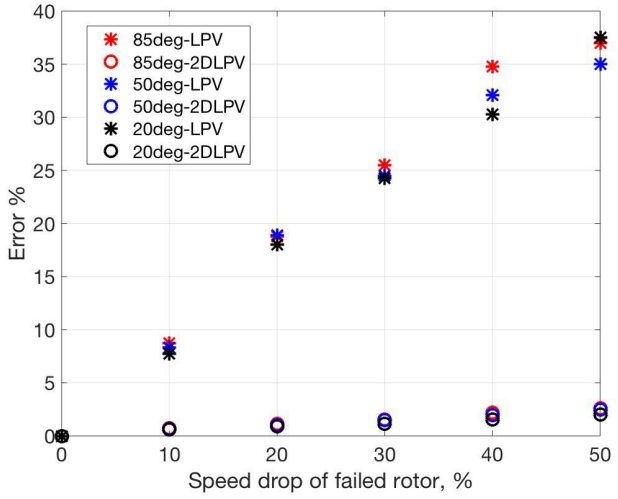

Fig. 3. Model error evaluation with mid-left rotor failure.

the approximated 2-D LPV model G_{2dlpv} can be evaluated by

$$\mathcal{E} = \left\| G_{trim}(s) - G_{2dlpv}(s) \right\|_{\sigma-2} / \left\| G_{trim}(s) \right\|_{\sigma-2}, \quad (30)$$

where σ is properly selected to make sure both $G_{2dlpv}(s+\sigma)$ and $G_{trim}(s+\sigma)$ are stable under the entire tilt-transition operation with rotor failure. Consider the rotor failure of either front-right and mid-left rotor with different rotor speed drop percentage at multiple transition stages (e.g., 85, 50 and 25 deg), the model error evaluation results are shown in Figs. 2 and 3, where the nominal LPV models are also evaluated for comparison. Note that some red circle markers in Figs. 2 and 3 are covered by these circles in other colors.

It can be observed that the modeling error of the 2-D LPV model are below 5%, and is slightly increased due to deviation of the rotor speed from its nominal condition. The improved model accuracy of the 2-D LPV model over the 1-D one can be observed clearly in Figs. 2 and 3. Note that the LPV model is obtained using the first order linearization of the nonlinear model (1) based on Taylor expansion by ignoring high order terms. For the case of tilt transition with single motor failure, there are two linear terms (tilt angle and rotor speed deviation from nominal speed trajectory) in the Taylor. The 1-D LPV model is obtained by setting speed deviation term to zero, which will have large modeling error than that of 2-D LPV using both terms.

4. ADAPTIVE MPC BASED ON 2-D LPV MODEL

Note that for the discrete-time affine LPV model stated in (10), $\Delta x(k+1)$ can be presented by

$$\Delta x(k+1) = x(k+1) - x_0(k+1) - \dot{x}_0(k+1)T, \quad (31)$$

and (10) can be put into the following form

$$\begin{aligned}\Delta x(k+1) = {} & A(\rho(k), \dot{\Gamma}(k))\Delta x(k) \\ & + B(\rho(k), \dot{\Gamma}(k))\Delta u(k). \end{aligned} \quad (32)$$

Let $e(k) = \Delta x_{ref} - \Delta x(k)$ represent the tracking error at current time step k, the adaptive MPC design method [30-32] is to find the constrained optimal control law $\Delta u(k)$ over a given horizon N that minimizes the constrained quadratic performance defined by

$$\begin{aligned}\min_{\Delta u(k),\ldots,\Delta u(k+N-1)} \frac{1}{2}\{ & \sum_{m=0}^{N} e^T(k+m)Qe(k+m) \\ & + \sum_{m=0}^{N-1} \Delta u^T(k+m)R\Delta u(k+m)]\} \end{aligned}$$

$$\text{subject to } G\Delta u(k+m) \le h,\ m = 0,\ \ldots,\ N-1, \quad (33)$$

where matrices $Q \ge 0$ and $R > 0$ are weightings for penalizing tracking error $e(k)$ and control effort $\Delta u(k)$, respectively; and matrix G is constraint to guarantee that control effort $\Delta u(k)$ stays within the prescribed bound h. Furthermore, vectors $e(k+m)$ and $\Delta u(k+m)$ represent the predicted error and control input at time step m. For a finite prediction horizon of N steps, the cost function and the constraint equation (33) can be put into the following compact form.

$$\begin{aligned}& \min_{\hat{u}(k)} \frac{1}{2}[\hat{e}^T(k)\hat{Q}\hat{e}(k) + \Delta\hat{u}^T(k)\hat{R}\Delta\hat{u}(k)] \\ & \text{subject to } \hat{G}\Delta\hat{u}(k) \le \hat{h}, \end{aligned} \quad (34)$$

where

$$\hat{e}(k) = \begin{bmatrix} e(k) \\ e(k+1) \\ \vdots \\ e(k+N) \end{bmatrix}, \ \Delta\hat{u}(k) = \begin{bmatrix} \Delta u(k) \\ \Delta u(k+1) \\ \vdots \\ \Delta u(k+N-1) \end{bmatrix},$$

$$\hat{h} = \left[h^T,\ h^T, \ldots,\ h^T\right]^T,$$
$$\hat{R} = block\ diag\left[R,\ R, \ldots,\ R\right],$$
$$\hat{G} = block\ diag\left[G,\ G, \ldots,\ G\right],$$
$$\hat{Q} = block\ diag\left[Q,\ Q, \ldots,\ Q\right]. \tag{35}$$

In addition, the prediction error (over the given horizon) $\hat{e}(k)$ can be defined by

$$\hat{e}(k) = \hat{A}e(k) + \hat{B}\Delta\hat{u}(k), \tag{36}$$

where

$$\hat{A} = \left[I\ \ A(k)^T\ \ A^2(k)^T\ \ \ldots\ \ A^N(k)^T\right]^T,$$
$$\hat{B} = \begin{bmatrix} 0 & 0 & \ldots & 0 \\ B(k) & 0 & \ldots & 0 \\ A(k)B(k) & B(k) & \ldots & 0 \\ \vdots & \vdots & \ddots & 0 \\ A^{N-1}(k) & A^{N-2}(k)B(k) & \ldots & B(k) \end{bmatrix}.$$

Equation (36) indicated that predicted tracking error $\hat{e}(k)$ can be calculated based on the current tracking error $e(k)$ and control vector $\Delta\hat{u}(k)$. As a result, utilizing the current information, the above optimization problem can be reformulated as below

$$\min_{\Delta\hat{u}(k)}\{\frac{1}{2}\Delta\hat{u}^T(k)(\hat{R}+\hat{B}^T\hat{Q}\hat{B})\Delta\hat{u}(k) + e^T(k)\hat{A}^T\hat{Q}\hat{B}\Delta\hat{u}(k) + \frac{1}{2}e^T(k)\hat{A}^T\hat{Q}\hat{A}e(k)\}$$
$$\text{subject to} \quad \hat{G}\Delta\hat{u}(k) \le \hat{h}(k). \tag{37}$$

It can be seen that control law $\Delta\hat{u}(k)$ as the solution of the above optimization problem is also optimal to the constrained optimization problem in (32) and (33).

Note that to obtain the real-time control at the current time step k for given the measured or estimated tracking error $e(k) = \Delta x_{ref} - \Delta x(k)$, the quadratic programming (QP) solver in Matlab [34] can be used to solve the optimization problem in (37). Instead of applying only the first control entry $\Delta u(k+0)$ at current time step k and repeating the optimization process for the next time step $k+1$, a control horizon of $N_c \le N$ is chosen so that the first N_c control entries $[u(k+0),\ u(k+1),\ ...,\ u(k+N_c-1)]$ are used between current time step k and time step $k+N_c-1$. Subsequently, the optimization process is repeated at time step $k+N_c-1$ to solve for the next control effort $[u(k+N_c),\ u(k+N_c+1),\ ...,\ u(k+2N_c-1)]$ [35].

4.1. Dynamic reference compensation (DRC)

Fig. 4 shows the proposed adaptive MPC strategy with a feedforward dynamic reference compensation (DRC) architecture, where Δx and Δu are the deviations of both controlled system states and inputs defined in Eq. (32). In this

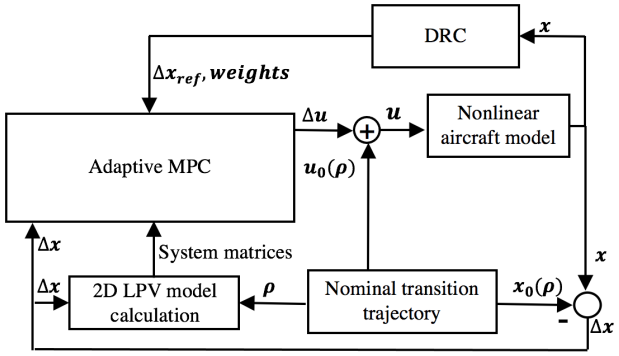

Fig. 4. The proposed adaptive MPC-DRC architecture.

study, the penalized tracking outputs are the forward speed Δx_2, vertical speed Δx_3, and pitch rate Δx_4, the reference vertical speed Δx_3^{ref} and reference pitch rate Δx_4^{ref} are adjusted based on the relevant state status (to be addressed later) while the reference vertical speed Δx_2^{ref} is kept at zero. Based on the real-time state reference signal Δx^{ref} and system state feedback signal Δx, the adaptive MPC law generates a set of optimized control signals $\Delta u(k+m)$, $m = 0,\ 1,\ ...,\ N-1$, from which the control signals within the control horizon, i.e., $[\Delta u(k)\ \ \cdots\ \ \Delta u(k+N_c-1)]$ and $N_c < N$, are selected as the optimal state-feedback control Δu and to be combined with the nominal control input $u_0(\rho)$ to form a complete control input, $u = \Delta u + u_0(\rho)$. In this study, all system states x are assumed to be measurable, and the required control feedback signal Δx is defined as $\Delta x = x - x_0(\rho)$, where $x_0(\rho)$ denotes the nominal state.

To follow the aircraft forward velocity during the initial tilt-transition, the dynamic reference compensation method [19] is proposed. Note that the forward velocity can be compensated by using a real-time reference pitch rate feedback defined below since the aircraft pitch rate is directly affected by the rotor thrust forces.

$$\Delta x_4^{ref} = G_1(\rho)\Delta x_2 - K_p\Delta x_8, \tag{38}$$

where Δx_2 is the forward velocity error and $G_1(\rho)$, function of $\rho(t)$, is the sensitivity gain for dynamic reference compensation. Therefore, to compensate for the forward velocity, a small weighting on the forward velocity error $Q_{[2,2]}(\rho)$ and a large sensitivity gain $G_1(\rho)$ at the beginning of transition flight are used in the MPC design. As the transition progresses, weighting $Q_{[2,2]}(\rho)$ increases gradually, while sensitivity gain $G_1(\rho)$ is reduced correspondingly as the fixed-wing aerodynamic effect becomes prominent. Using the same principle, the aircraft pitch attitude control is achieved by adjusting the reference angular speed based on the feedback angular position multiplied by a tunable gain K_p. Therefore, the combined reference pitch rate can be given by (38). In summary, the desired forward velocity tracking can be achieved by ad-

justing reference pitch rate as a function of velocity error and pitch attitude, along with an increased penalty on forward velocity error depending on $\rho(t)$.

Similarly, to maintain the desired flight altitude during tilt-transition, vertical reference speed is compensated using altitude error Δx_{12} defined below

$$\Delta x_3^{ref} = -K_v \Delta x_{12}, \tag{39}$$

where K_v is the sensitivity gain.

5. SIMULATION INVESTIGATION

5.1. Reference articulation trajectory

In this simulation study, the mid-rotor tilting speed is given at 2 deg/s, which means that there are 45 seconds for tilting from vertical (90 deg) to horizontal position (0 deg). The aircraft is required to be maintained at certain designated altitude subject to attitude-hold with zero vertical and lateral velocities, with the forward speed constantly accelerated from zero to the target cruising speed (68 m/s). Noting that the simulation duration is set to 50 seconds for validating the converged performance.

5.2. Transition with front-right motor failure

Firstly, it is assumed that the available front right motor power failed to 50% of hovering power, which is a 60% motor power loss considering the peak motor power $P_{max} = 1.25P_{hover}$. In order to validate the capability of the proposed 2D-LPV modeling and control method, a 1-D LPV-MPC was developed which does not take motor failure into consideration. But its design weighting is also optimized based on the same procedure. Based on control parameters defined in Table 3, the closed-loop simulation results are presented below, where the level flight speed V_y, pitch angle α and vertical speed V_z are shown in Fig. 5.

It is obvious that oscillations for all system outputs are reduced under 2D-LPV model based control. This is mainly due to the fact that for the 1-D LPV-MPC, the system model used in control design is not able to capture the

Table 3. Adaptive MPC-DRC controller parameters.

Parameter	Value
$Q_{[2,2]}$	$G_2(\rho)$
$Q_{[3,3]}$	200^2
$Q_{[4,4]}$	4000^2
$R_{[1:6,1:6]}$	$0.01^2 \times I_6$
$R_{[9,9]}$	0.01^2
Step size, ms	1
Prediction Horizon	4
Control Horizon	2
Δx_3^{ref}	$-\Delta x_{12}$
Δx_4^{ref}	$-\Delta x_8 + G_1(\rho)\Delta x_2$

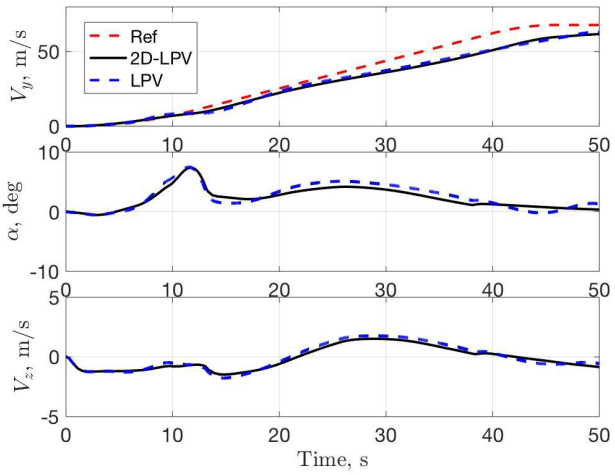

Fig. 5. Simulation responses of tilt- transition with front-right motor failure.

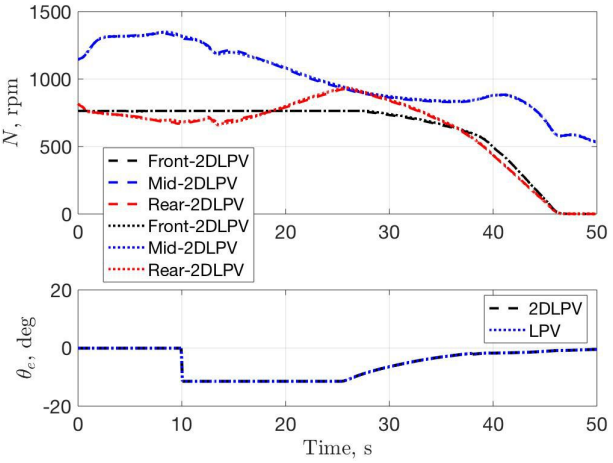

Fig. 6. Control efforts of transition with front-right motor failure.

aircraft dynamics variation caused by the motor failure but 2-D LPV-MPC does. Regarding the transition control performance, it can be observed that the aircraft completes its tilting process and reaches the target level speed at the end of 50s. However, the vertical speed drops at the beginning of tilting process since the lift thrusts are limited due to the rotor failure. Also, the aircraft is holding a positive pitch angle during the transition, which is due to the dynamic reference compensation. With the increased aircraft longitudinal speed, the pitch up motion transfers the aircraft to a climbing pose to compensate for the altitude drop. On the other side, the level flight speed tracking performance is also sacrificed due to the climbing pose. The rotor speed and elevator deflection are shown in Fig. 6.

The vehicle roll and yaw motions can still be balanced with left and right symmetric propeller thrusts. With the front rotor speed dropping due to the failure, the rear ro-

tor speed was reduced to balance the aircraft pitch motion. The elevator control is activated after 10 sec with the effective aerodynamics generated from the increased level flight speed.

5.3. Transition with mid-right motor failure

Following the same procedure of investigating the front-right motor failure in the above subsection, the mid-right motor failure is studied with the simulation results shown in Fig. 7.

At the initial stage, the level flight tracking performance is relatively poor because of insufficient failed tilt-rotor thrust. After a quick pitching up, the aircraft keeps pitching down between 15 and 38 sec, which brings the thrust vector of untilted front and rear rotor toward the front to compensate the level flight acceleration. The rotor speed and elevator deflection are shown in Fig. 8, where the front

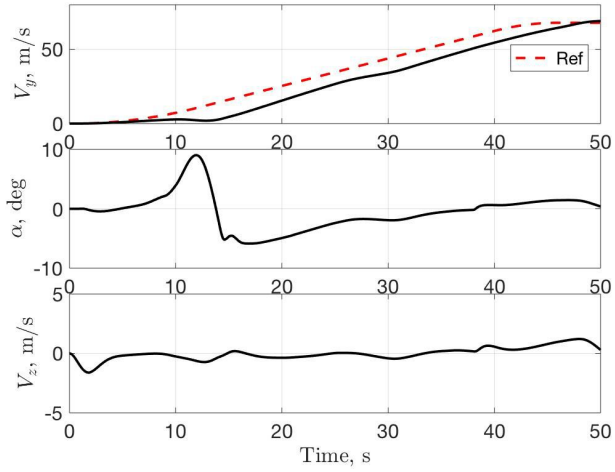

Fig. 7. Simulation responses of transition with mid-right motor failure.

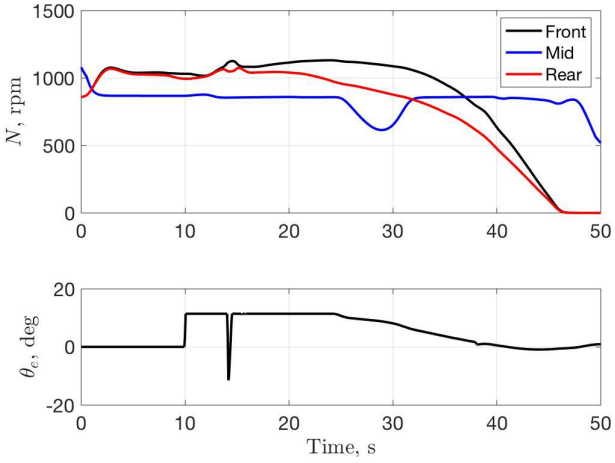

Fig. 8. Control effort of transition with mid-right motor failure.

and rear rotors are operated at high speed to hold the aircraft at desired altitude due to lack of lift force from the reduced mid rotor thrust and slower longitudinal speed than the reference one (resulting in decreased wing lift). Finally, at the 50th sec, the aircraft completes the transition process with the targeted cruising speed reached.

In this study, the MPC design complexity is significantly reduced by using dynamic compensation method stated in Subsection 4.1 to reduce the computational throughput. All studies are simulated using Matlab Version 2019b running on a MacBook Pro equipped with a 2.2 GHz Intel Core i7 processor. The run-time for a 20 second flight simulation with both adaptive MPC strategy and nonlinear aircraft model is about 12 seconds. This is considered acceptable for real-time implementation since simulation time is significantly shorter than the actual one even included the nonlinear aircraft model.

6. CONCLUSION

This paper presents a tilt-transition modeling and control method for a six-rotor eVTOL (electric vertical take-off and landing) aircraft with two tiltable middle rotors under single rotor failure. Based on the nonlinear aircraft model developed earlier, an online identified 2-D LPV modeling method has been developed, considering the aircraft dynamic characteristics with improved the reference model accuracy. The σ shifted $\mathcal{H}_2$ norm is introduced and used for evaluating the 2-D LPV model error caused by online updated LPV model. Then, adaptive MPC method is used to design the transition control strategy with time-varying hard constraints and dynamic reference compensation. Simulation case studies were conducted and show that the 2-D LPV model-based MPC scheme is robust to the rotor failure conditions during the transition process. In summary, this paper demonstrates the effectiveness of adaptive MPC scheme based on 2-D online updated LPV model to achieve desired tilt-transition performance under single motor failure. Note that If multiple rotors are failed one by one, it is expected that the proposed method can be expanded to stabilize aircraft based on a higher dimension LPV model than two if the lift generated by rotors and wing is greater than the aircraft weight. The future work is to study a) extension of LPV model with multiple rotor failures, b) aircraft failure MPC control with emergency landing trajectory planning based on online updated LPV model, and c) development of MPC control with guaranteed stability.

REFERENCES

[1] J. Holden and N. Goel, "Uber elevate: Fast-forwarding to a future of on-demand urban air transportation," 2016.

[2] R. Binder, L. Garrow, B. German, P. Mokhtarian, M. Daskilewicz, and T. Douthat, "If you fly it, will commuters

come? predicting demand for evtol urban air trips," in *Proc. of AIAA Conference*, Atlanta, Georgia, pp. 1-41, 2018.

[3] G. E. Dorrington *et al.*, "Performance of electric vertical take-off and landing (evtol) hovering craft," in *Proc. of AIAC18: 18th Australian International Aerospace Congress (2019): HUMS-11th Defence Science and Technology (DST) International Conference on Health and Usage Monitoring (HUMS 2019): ISSFD-27th International Symposium on Space Flight Dynamics (ISSFD)*, Engineers Australia, Royal Aeronautical Society, p. 84, 2019.

[4] I. C. Kleinbekman, M. A. Mitici, and P. Wei, "evtol arrival sequencing and scheduling for on-demand urban air mobility," in *Proc. of 2018 IEEE/AIAA 37th Digital Avionics Systems Conference (DASC)*, IEEE, pp. 1-7, 2018.

[5] B. German, M. Daskilewicz, T. K. Hamilton, and M. M. Warren, "Cargo delivery in by passenger evtol aircraft: A case study in the san francisco bay area," in *2018 AIAA Aerospace Sciences Meeting*, p. 2006, 2018.

[6] P. Pradeep and P. Wei, "Heuristic approach for arrival sequencing and scheduling for evtol aircraft in on-demand urban air mobility," in *2018 IEEE/AIAA 37th Digital Avionics Systems Conference (DASC)*, IEEE, pp. 1-7, 2018.

[7] T. Lombaerts, J. Kaneshige, S. Schuet, G. Hardy, B. L. Aponso, and K. H. Shish, "Nonlinear dynamic inversion based attitude control for a hovering quad tiltrotor evtol vehicle," in *Proc. of AIAA Scitech 2019 Forum*, p. 0134, 2019.

[8] M. Skuhersky, *A First-principle Power and Energy Model for eVTOL Vehicles*, Ph.D. dissertation, 2019.

[9] P. Pradeep and P. Wei, "Energy efficient arrival with RTA constraint for urban evtol operations," in *Proc. of 2018 AIAA Aerospace Sciences Meeting*, p. 2008, 2018.

[10] M. Daskilewicz, B. German, M. Warren, L. A. Garrow, S.-S. Boddupalli, and T. H. Douthat, "Progress in vertiport placement and estimating aircraft range requirements for eVTOL daily commuting," in *Proc. of 2018 Aviation Technology, Integration, and Operations Conference*, p. 2884, 2018.

[11] P. Payuhavorakulchai, "Cost analysis of evtol configuration design for air ambulance in japan," 2019.

[12] J. M. Vegh, E. Botero, M. Clarke, J. Smart, and J. Alonso, "Current capabilities and challenges of ndarc and suave for evtol aircraft design and analysis," in *Proc. of AIAA Propulsion and Energy 2019 Forum*, p. 4505, 2019.

[13] S.-S. Boddupalli, *Estimating Demand for an Electric Vertical Landing and Takeoff (eVTOL) Air Taxi Service Using Discrete Choice Modeling*, Ph.D. dissertation, Georgia Institute of Technology, 2019.

[14] P.-M. Basset, B. D. Vu, P. Beaumier, G. Reboul, and B. Ortun, "Models and methods at onera for the presizing of evtol hybrid aircraft including analysis of failure scenarios," 2018.

[15] J. Zhang, S. Liguo, Q. Xiangju, and W. Liuping, "Time-varying linear control for tiltrotor aircraft," *Chinese Journal of Aeronautics*, vol. 31, no. 4, pp. 632-642, 2018.

[16] R. T. Rysdyk and A. J. Calise, "Adaptive model inversion flight control for tilt-rotor aircraft," *Journal of guidance, control, and dynamics*, vol. 22, no. 3, pp. 402-407, 1999.

[17] X. Wang and L. Cai, "Mathematical modeling and control of a tilt-rotor aircraft," *Aerospace Science and Technology*, vol. 47, pp. 473-492, 2015.

[18] E. Cetinsoy, S. Dikyar, C. Hançer, K. Oner, E. Sirimoglu, M. Unel, and M. Aksit, "Design and construction of a novel quad tilt-wing UAV," *Mechatronics*, vol. 22, no. 6, pp. 723-745, 2012.

[19] S. Qu, G. Zhu, W. Su, and S. S. Swei, "LPV-based transition flight control design for a tilt-rotor aircraft," *Proceedings of IMechE, Part G: Journal of Aerospace Engineering*, vol. 236, no. 16, pp. 3354-3369, 2022.

[20] W. Su, S. Qu, G. G. Zhu, S. S.-M. Swei, M. Hashimoto, and T. Zeng, "A control-oriented dynamic model of tiltrotor aircraft for urban air mobility," in *Proc. of AIAA Scitech 2021 Forum*, p. 0091, 2021.

[21] J. S. Shamma, "An overview of LPV systems," in *Control of Linear Parameter Varying Systems with Applications*, Springer, pp. 3-26, 2012.

[22] S. Qu, T. He, and G. G. Zhu, "Engine EGR valve modeling and switched LPV control considering nonlinear dry friction," *IEEE/ASME Transactions on Mechatronics*, 2020.

[23] S. Qu, T. He, and G. G. Zhu, "LPV modeling and switched control for EGR valves with dry friction," in *Proc. of 2019 IEEE Conference on Control Technology and Applications (CCTA)*, IEEE, pp. 400-405, 2019.

[24] T. He, G. G. Zhu, S. S.-M. Swei, and W. Su, "Smooth-switching LPV control for vibration suppression of a flexible airplane wing," *Aerospace Science and Technology*, vol. 84, pp. 895-903, 2019.

[25] T. He, A. K. Al-Jiboory, G. G. Zhu, S. S.-M. Swei, and W. Su, "Application of ICC LPV control to a blended-wing-body airplane with guaranteed hinf performance," *Aerospace Science and Technology*, vol. 81, pp. 88-98, 2018.

[26] H. Fukushima, T.-H. Kim, and T. Sugie, "Adaptive model predictive control for a class of constrained linear systems based on the comparison model," *Automatica*, vol. 43, no. 2, pp. 301-308, 2007.

[27] J.-S. Kim, "Recent advances in adaptive MPC," in *Proc. of ICCAS 2010*, IEEE, pp. 218-222, 2010.

[28] B. Ding, "Dynamic output feedback mpc for lpv systems via near-optimal solutions," in *Proc. of the 30th Chinese Control Conference*, IEEE, pp. 3340-3345, 2011.

[29] A. Casavola, D. Famularo, and G. Franze, "A feedback min-max mpc algorithm for lpv systems subject to bounded rates of change of parameters," *IEEE Transactions on Automatic Control*, vol. 47, no. 7, pp. 1147-1153, 2002.

[30] E. F. Camacho and C. B. Alba, *Model Predictive Control*, Springer Science & Business Media, 2013.

[31] D. Q. Mayne, J. B. Rawlings, C. V. Rao, and P. O. Scokaert, "Constrained model predictive control: Stability and optimality," *Automatica*, vol. 36, no. 6, pp. 789-814, 2000.

[32] C. E. Garcia, D. M. Prett, and M. Morari, "Model predictive control: theory and practice-A survey," *Automatica*, vol. 25, no. 3, pp. 335-348, 1989.

[33] A. K. Al-Jiboory, G. Zhu, S. S.-M. Swei, W. Su, and N. T. Nguyen, "LPV modeling of a flexible wing aircraft using modal alignment and adaptive gridding methods," *Aerospace science and technology*, vol. 66, pp. 92-102, 2017.

[34] C. Schmid and L. T. Biegler, "Quadratic programming methods for reduced hessian sqp," *Computers & Chemical Engineering*, vol. 18, no. 9, pp. 817-832, 1994.

[35] T. H. Phuong, M. P. Belov, and D. Van Thuy, "Adaptive model predictive control for nonlinear elastic electrical transmission servo drives," in *Proc. of 2019 IEEE Conference of Russian Young Researchers in Electrical and Electronic Engineering (EIConRus)*, IEEE, pp. 704-708, 2019.

Shen Qu is currently a software engineer in vehicle dynamics at TuSimple, San Diego, CA, USA. He received double B.S. degree in automotive engineering from Beijing Institute of Technology, Beijing, China, in 2016 and in mechanical engineering from Polytechnic University of Turin, Turin, Italy in 2016. His Ph.D. degree in 2021 is with the department of Mechanical Engineering, Michigan State University, East Lansing, MI, USA. His research interests include model predictive control, linear parameter varying control and system modeling and control optimization with applications to both automotive and aerospace engineering.

Guoming Zhu is currently a Gardner endowed chair and professor with the Department of Mechanical Engineering, Michigan State University, East Lansing, MI, USA. He received the B.S. and M.S. degrees from the Beijing University of Aeronautics and Astronautics, Beijing, China, in 1982 and 1984, respectively, and the Ph.D. degree in aerospace engineering from Purdue University, West Lafayette, IN, USA, in 1992. He was a Technical Fellow in advanced powertrain systems with Visteon Corporation, and a Technical Advisor with Cummins Engine Co., Ltd. Dr. Zhu has authored or co-authored over 280 refereed technical papers, two books, and more than 40 U.S. patents. Dr. Zhu is a Fellow of the SAE and ASME. He is an Editorial Board Member of the International Journal of Powertrain. He was the program chair of the 2018 ASME Dynamic Systems and Control Conference and an Associate Editor of the ASME Journal of Dynamic Systems, Measurement, and Control.

Weihua Su is currently an associate professor with the Department of Aerospace Engineering and Mechanics, The University of Alabama, Tuscaloosa, AL, USA. He received the B.S. and M.S. degrees from the Beijing University of Aeronautics and Astronautics, Beijing, China, in 2000 and 2002, respectively, and the Ph.D. degree in aerospace engineering from The University of Michigan, Ann Arbor, MI, USA, in 2008. Dr. Su has authored or co-authored over 70 refereed technical papers. Dr. Su is an elected member of both the Structural Dynamics Technical Committee of AIAA and the Structures and Materials Technical Committee of ASME.

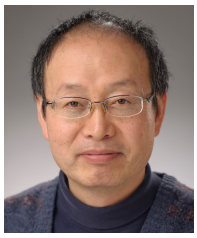

Sean Shan-Min Swei was formerly with NASA Ames Research Center and is currently a Professor of Practice in the Department of Aerospace Engineering at Khalifa University (KU), Abu Dhabi, UAE, and Director of KU Space Technology and Innovation Center (KUSTIC). He received the BSc in Mechanical Engineering from National Taiwan University in 1983, MSc in Mechanical Engineering and Mechanics from Drexel University in 1986, and Ph.D. in Aeronautics and Astronautics from Purdue University in 1993. Dr. Swei's main research interests are in the general areas of air and spaceflight vehicle systems, space structures and their integration with advanced autonomous/robotic systems.